Catalysis Science & Technology

ROYAL SOCIETY OF CHEMISTRY

PAPER

View Article Online
View Journal

Cite this: DOI: 10.1039/d6cy00216a

Nickel catalysts in the hydrogenation of benzyltoluene using impure hydrogen streams

Lukas Popp and Patrick Schühle *

Biomass-derived hydrogen is frequently contaminated with CO and CO_2, which limits its direct utilization in downstream applications. Cyclic hydrogenation/dehydrogenation of liquid organic hydrogen carriers (LOHCs) such as benzyltoluene (BT) provides a pathway to simultaneously store hydrogen and purify such "low-grade" hydrogen feeds. In this context, Ni-based catalysts are particularly attractive because they can hydrogenate aromatic systems under CO-containing atmospheres while representing a relatively cheap alternative to noble metal catalysts. Here, we systematically investigate BT hydrogenation over a commercial $Ni/Al_2O_3/SiO_2$ catalyst under process-relevant LOHC conditions (T = 170–230 °C, p = 10–50 bar) in the presence of CO (0–6%) and demonstrate that BT conversion remains feasible even at high CO levels, while the hydrogenation rate decreases due to competitive CO adsorption. Time-resolved analysis of both gas- and liquid-phase compositions further reveals CO methanation during BT hydrogenation, indicating that both reactions proceed in parallel while competing for active sites. By varying temperature and total pressure, the balance between BT hydrogenation and methanation can be steered, with 230 °C and 50 bar identified as the most favorable conditions for efficient BT hydrogenation under CO presence. In addition, introducing CO_2 at biomass-typical concentrations (30 vol%) shows that it likewise adsorbs competitively on Ni and is also converted to methane. Collectively, these results highlight Ni-based catalysts as a robust catalyst for mixed-gas hydrogenation and LOHC-enabled purification/storage of biogenic hydrogen, while underscoring an inherent trade-off between competitive (co-)methanation, that consumes a fraction of hydrogen as CH_4 that cannot be recovered upon LOHC dehydrogenation, yet constitutes an energy-dense coproduct stream that may be valorized.

Received 20th February 2026,
Accepted 7th April 2026

DOI: 10.1039/d6cy00216a

rsc.li/catalysis

Introduction

The conversion of waste-derived biomass into hydrogen is emerging as a pivotal strategy in the transition to a sustainable, circular energy economy.[1–3] This approach leverages biogenic residues, such as agricultural by-products, organic waste, sewage sludge, and forestry residues, thereby mitigating the competition with food production and contributing to carbon-neutral hydrogen production.[4–7]

The gas mixture resulting from biomass conversion, *e.g.* by gasification, predominantly comprises hydrogen (H_2), carbon monoxide (CO), carbon dioxide (CO_2), methane (CH_4), and nitrogen (N_2).[8–10] While hydrogen is the desired energy carrier, the presence of these impurities poses significant challenges for its direct utilization in, *e.g.*, fuel cell applications. Carbon monoxide is a potent catalyst poison, even at low concentrations, leading to irreversible deactivation of platinum- or nickel-based catalysts in membrane fuel cells (PEMFCs and HEMFCs).[11–14] Carbon dioxide acts on the one hand as an inert diluent, reducing the hydrogen partial pressure and thereby decreasing the electrochemical conversion efficiency.[15,16] On the other hand, certain catalysts can promote the formation of CO from CO_2 in the presence of hydrogen, for example, *via* the reverse water-gas shift reaction.[17] Methane, formed during incomplete reforming or at low temperatures, increases the calorific value of the gas but is unsuitable for direct fuel cell utilization and requires additional processing, such as steam reforming, to release usable hydrogen.[10] Nitrogen, introduced during, *e.g.* air-based gasification, significantly dilutes the syngas and does not participate in electrochemical reactions, further reducing the energy density per unit volume and complicating downstream processing.[18,19] Conventional hydrogen purification methods such as pressure swing adsorption (PSA), cryogenic separation, and chemical scrubbing are energy-intensive and costly.[20,21] PSA alone typically cannot achieve PEM fuel cell-grade hydrogen purity (>99.0%) and therefore, requires additional purification steps.[22–24] Cryogenic separation demands substantial refrigeration energy, while chemical scrubbing involves continuous reagent consumption and added operational

Institute of Chemical Reaction Engineering, Friedrich-Alexander-Universität, Erlangen-Nürnberg, 91058 Erlangen, Germany. E-mail: patrick.schuehle@fau.de

complexity.[25] These technologies also perform poorly under fluctuating gas compositions typical of biomass-derived streams.[26,27] High capital and operating costs along with multi-stage process integration limit their suitability for small- and medium-scale decentralized biomass-to-hydrogen applications.[22,24] Hydrogen purification can also be accomplished through cyclic hydrogenation/dehydrogenation of unsaturated hydrocarbons. In this process, hydrogen present in a mixed gas stream is selectively bound covalently to a liquid carrier *via* catalytic hydrogenation, while accompanying impurities are removed through the gas phase (see Fig. 1). Subsequent catalytic dehydrogenation enables the recovery of hydrogen in high purity, and the carrier liquid is regenerated for repeated use, forming the cyclic process. Liquid organic hydrogen carriers (LOHCs), so far investigated for hydrogen storage and transportation, can consequently also be applied to accomplish hydrogen purification. Among these organic carriers, benzyltoluene (BT) has emerged as an especially promising substance due to its high hydrogen storage capacity, favourable hazard profile, wide liquid-phase temperature range and commercial availability on a large scale. Hydrogen-lean BT (H0-BT) is converted to its hydrogen-rich form perhydro-benzyltoluene (H12-BT) *via* catalytic hydrogenation at 150–180 °C and 20–30 bar hydrogen pressure.[28,29] Subsequent catalytic dehydrogenation at 280–300 °C near atmospheric pressure enables the recovery of hydrogen in high purity, while the benzyltoluene carrier is regenerated for repeated use.[30–32]

In direct hydrogenation of liquid carriers with impure hydrogen (mixed gas hydrogenation), the gas phase contains H_2, CO, and CO_2, which can undergo the (reverse) water-gas shift reaction (1) and methanation reaction (2) and (3) in parallel.[33]

$$CO + H_2O \rightleftharpoons CO_2 + H_2 \quad (1)$$

$$CO + 3H_2 \rightleftharpoons CH_4 + H_2O \quad (2)$$

$$CO_2 + 4H_2 \rightleftharpoons CH_4 + 2H_2O \quad (3)$$

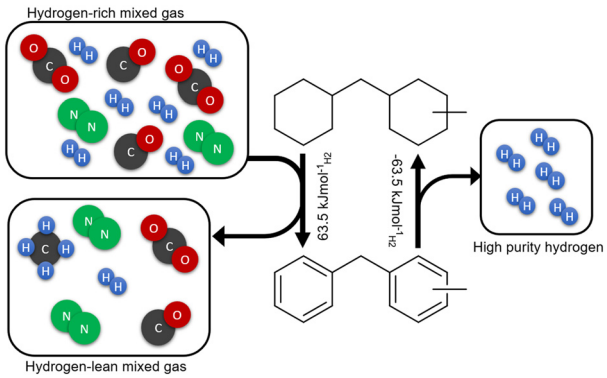

Fig. 1 (De)hydrogenation cycle to purify hydrogen with the use of benzyltoluene as a purification liquid.

These processes alter the hydrogen partial pressure and gas composition near the liquid–gas interface, thereby influencing hydrogen availability for the LOHC hydrogenation. Depending on operating conditions and catalyst, the extent of these gas-phase conversions can significantly affect the overall hydrogen utilization efficiency.[34,35] Understanding these coupled gas-phase reactions is therefore essential for optimizing the performance and selectivity of mixed-gas LOHC hydrogenation systems. The hydrogenation process is typically catalysed by noble metals like Pt or Pd, due to their superior activity and selectivity.[32,36,37] However, these noble metal catalysts are highly susceptible to impurities—especially CO—which strongly adsorb on active sites and severely reduce hydrogenation efficiency. Recent investigations on LOHC systems by Jorschick *et al.* demonstrated that Pd/Al_2O_3 maintains BT hydrogenation activity in gas mixtures containing low amounts of CO and CO_2, while Pt centres are completely poisoned under the applied conditions.[38] Seitz *et al.* found that phosphate modification of Pd/Al_2O_3 significantly enhances catalytic activity and stability in aromatic hydrogenation under CO-contaminated hydrogen, attributing this to the expression of poisoning-resistant Pd sites due to small particle diameters.[39] Nickel represents a valid alternative to Pd for hydrogenation catalysts: economically, Ni is orders of magnitude less expensive than Pd, and catalytically, Ni-based catalyst have demonstrated competitive activity in the hydrogenation of aromatic compounds.[40] Moreover, when used in tandem with noble metals, these systems exhibit enhanced resistance to CO poisoning while maintaining high hydrogenation performance.[41] Regarding the performance under a CO-containing atmosphere, liquid-phase naphthalene hydrogenation was investigated by Sekine *et al.* over a supported Ni catalyst, showing that Ni retains measurable aromatic hydrogenation activity despite CO adsorption and concurrent CO hydrogenation.[42] Additionally, Le *et al.* evaluated Ni/SiO_2 catalysts using benzene hydrogenation alongside CO methanation to assess Ni functionality for aromatic saturation alongside CO conversion under process-relevant conditions.[43]

In this study, the hydrogenation of benzyltoluene in the presence of CO- and CO_2-containing hydrogen gas mixtures is demonstrated by using a commercial nickel-based catalyst. The effects of temperature, total pressure, and the partial pressures of the aforementioned impurities on H0-BT conversion, selectivity and stability are discussed. The progression of gas and liquid phase composition is monitored to enable a comprehensive understanding of the parallel reaction pathways.

Experimental

Materials

All chemicals were commercially sourced and utilized without additional purification. A nickel, silica and alumina

extrudate ($Ni/Al_2O_3/SiO_2$, loading 50 wt%, Clarinat®) was used as the hydrogenation catalyst. H0-Benzyltoluene (Hydrogenious Technologies®) is used as the LOHC. For the hydrogenation experiments, hydrogen (H_2, Air Liquide, 99.99%), a carbon monoxide/hydrogen mixture (2% CO in H_2, Air Liquide; 99.99%), carbon dioxide (CO_2, Air Liquide, 99.99%), nitrogen (N_2, Air Liquide, 99.99%) and argon (Ar, Air Liquide, 99.99%) were used as reaction gases. Liquid samples were dissolved in acetone (C_3H_6O, ≥99.8%, Merck KGaA) for further analysis. Chemicals used for catalyst characterization are mentioned below.

Catalyst characterisation

The crystal structure of the catalyst was investigated using powder X-ray diffraction (XRD). The measurements were carried out in angles of 10–90° 2θ, a scanning speed of 0.02° s^{-1}, a step size of 0.015° and 100 s time per step on an X'Pert Pro diffractometer (Malvern Panalytics). Cu-Kα was used as the radiation source and X'Celerator as the detector. The data were processed utilizing X'Pert HighScore Plus software and compared to simulated reflexes from the Inorganic Crystal Structure Database (ICSD). The elemental composition of the catalysts was measured *via* inductively coupled plasma-optical emission spectroscopy (ICP-OES). Approximately 100 mg of the samples were dissolved using microwave-assisted digestion at 220 °C in a solution containing HCl (32%; Merck KGaA), HNO_3 (65%, Merck KGaA) and HF (40%, Merck KGaA) (6 : 2 : 2 ml). The solutions were measured in an ICP-OES Ciros CCD (Spectro Analytical Instruments GmbH). The instrument was calibrated using standard nickel-containing solutions (nickel ICP standard, based on nickel(II) nitrate; Merck KGaA). Three consecutive measurements of the dissolved samples were carried out, and an average value was calculated. The surface area and the pore volume of the catalysts were determined by N_2-sorption on a Quantachrome Quadrasorb SI-MP-8 instrument. The samples were degassed at approximately 2×10^{-5} bar for 12 h at 250 °C. The relevant values were determined by applying the Brunauer–Emmett–Teller (BET) theory. H_2 temperature-programmed reduction (H_2-TPR) was performed on a Thermo Scientific TPDRO 1100 instrument (Thermo Electron Corporation). During the measurement, the sample was heated to a final temperature of 600 °C at a rate of 5 °C min^{-1} under a hydrogen flow of 20 cm^3 min^{-1}.

As this work aimed to assess the effect of CO on H0-BT hydrogenation in an industrially relevant system, a commercially available technical nickel catalyst was deliberately chosen to demonstrate a catalyst concept with practical potential for mixed-gas hydrogenation rather than to develop or optimize a model catalyst. For this reason, the characterization of the commercial catalyst was intentionally restricted to XRD, ICP-OES, N_2 physisorption and H_2-TPR. These methods were considered sufficient to identify the crystalline phases, determine the bulk Ni content, describe the textural properties and guarantee a reduced and active Ni under reaction conditions which were deemed relevant for reproducibility and comparison of catalytic results. A more detailed analysis of morphology, dispersion, and metal–support interaction by methods such as XPS, TEM or *in situ* DRIFT measurements was beyond the scope of the present study. Notably, in-depth characterization of supported Ni catalysts on Al_2O_3 and SiO_2 is intensively reported in the literature, whereas activity loss due to sintering, coking or phase changes are recorded at temperatures >300 °C.[44–49]

Hydrogenation experiments

Hydrogenation experiments were carried out in a 300 mL batch autoclave (Parr type 4566) equipped with a four-blade gas-inducing stirrer, an electric heating mantle, and a cooling coil connected to a cryostat (Huber Unichiller 022). The setup also included a type J thermocouple, a pressure recorder (Ashcroft type G2), and a process controller (Parr type 4875). A liquid sampling line fitted with a filter and needle valve (Nova Swiss) and a loop for continuous gas sampling were utilized. After the initial loading with 100 g H0-BT and Ni catalyst in an $n_{Ni} : n_{H0\text{-}BT}$ ratio of 0.045 the reactor was sealed with a Kalrez© 4079 O-ring and the setup was purged multiple times with Ar. The reactor was subsequently heated to a reaction temperature between 170 and 230 °C while stirring at 450 rpm. After the desired temperature was reached, the liquid sample line was flushed with 1 ml reaction solution. 30 bar CO/H_2 mixture was introduced to the reactor and 20 bar pure H_2 was added to reach the desired 50 bar hydrogenation pressure. Experiments were conducted in dead-end mode, maintaining constant H_2 pressure by continuously supplying H_2 to compensate for its consumption during the reaction. The reaction was initiated by increasing the stirrer speed stepwise to 1200 rpm, ensuring sufficient gas entrainment as well as mixing of the catalyst and the reaction fluids. The intervals for liquid and gas sampling are listed in Table S1. In additional experiments 15 bar CO/H_2 mixture was replaced by 15 bar either CO_2 or N_2. The step of adding a third gas was carried out after the target temperature had been reached. 30 µl of liquid sample were dissolved in 1 ml acetone and analysed *via* gas chromatography (Shimadzu GC-2010 Plus, FID, Restek Rxi-17Sil column). Calibration of the BT peaks in their different hydrogenation states is described elsewhere.[37] The gas samples were analysed *via* gas chromatography with coupled mass spectroscopy (Shimadzu Nexis GC-2030, FID, TCD, HAYESEP N60/80 precolumn, ShinCarbon main column). The calculation of performance parameters conversion, selectivity, degree of hydrogenation and molar hydrogen utilization is listed in the SI.

Results and discussion

Impact of CO content in hydrogenation gas

A series of experiments was conducted using a $Ni/Al_2O_3/SiO_2$ catalyst with varying CO content in hydrogen to study its

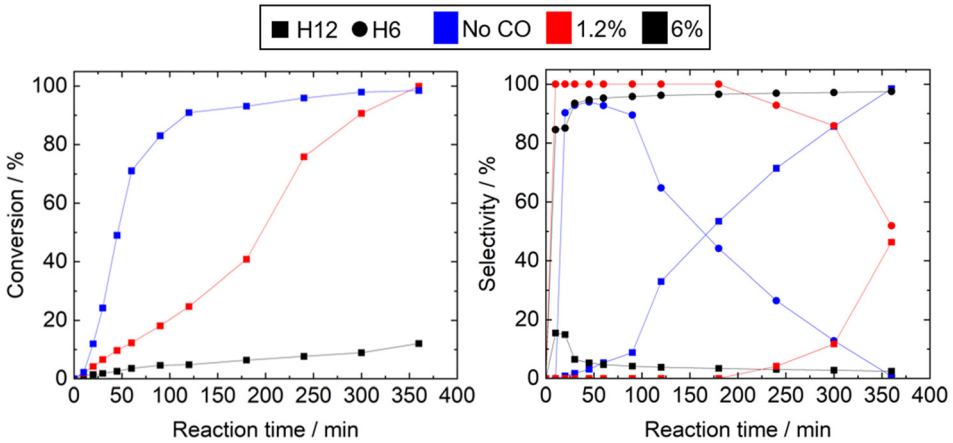

Fig. 2 Conversion (left) and selectivity (right) of benzyltoluene hydrogenation using a commercial nickel catalyst without CO impurities (blue), with 1.2% CO gas fraction (red) and 6% CO gas fraction (black) (reaction conditions: Ni/BT ratio 0.045, m_{BT} = 100 g, T = 170 °C, t = 6 h; p = 50 bar).

influence on BT conversion and selectivity towards fully hydrogenated H12-BT. CO fractions in the feed gas of 1.2% and 6% were adjusted and compared to a CO-free benchmark experiment. The results presented in Fig. 2 display the conversion (left) and the selectivity (right) for the hydrogenation with different CO concentrations at 170 °C. Comparison of the turnover after 6 h reaction time reveals that a substantially lower conversion of 12.1% was obtained at a CO gas fraction of 6%. Nearly all active sites on the catalyst are occupied by competitively adsorbed CO, leading to a pronounced suppression of BT hydrogenation activity. For the experiments without CO and at 1.2% CO gas fraction, almost full conversion of H0-BT can be achieved after 6 h reaction time. In contrast to the CO-free experiment, the introduction of 1.2% CO gas fraction results in a markedly reduced initial hydrogenation rate. After approximately 3 h of reaction time, a nearly exponential increase in hydrogenation activity is observed, followed by a slower approach to full conversion state. Although complete conversion is achieved in both cases, the presence of CO significantly delays the overall hydrogenation process, as reflected by a substantially lower DoH of 72.2% compared to 97.4% for pure H_2. A further increase in CO content results in a DoH of 6.4%. Table 1 lists the composition of the C1 components in the gas phase after 6 h reaction time. The results support the presence of a parallel reaction pathway by hydrogenation of CO to methane occurring alongside BT hydrogenation.[50] On the one hand, this additional hydrogen consumption and competition for active sites may contribute to the reduced hydrogenation rate. However, the partial CO conversion (mainly to methane and to a lesser degree to CO_2) gradually liberates the catalyst surface and makes it available for ongoing BT hydrogenation. The enhanced hydrogenation rate observed in the experiment with 1.2% CO gas fraction after 3 h might be due to reduced CO-induced blocking of active sites. Regarding the catalyst stability, no loss of active metal or reduction of surface area could be detected post reaction (see Table S2). At the beginning of the reaction, the nickel catalyst is still covered by a superficial oxide layer. It was previously reported that this oxide layer is removed under reaction conditions during the hydrogenation.[51] After the reaction and handling of the catalyst under ambient air and subsequent washing, this oxide layer reforms on the catalyst surface (see Fig. S14 and S15). H_2-TPR measurements suggest that the catalyst is present predominantly in its reduced state under the applied reaction conditions, as the observed reduction peaks occur within the temperature window of 150–250 °C, which overlaps with the reaction temperature range (see Fig. S16).

Table 1 Composition of the C1 components of the gas phase of benzyltoluene hydrogenation using a commercial nickel catalyst without CO impurities, with 1.2% and 6% CO gas fraction (reaction conditions: Ni/BT ratio 0.045, m_{BT} = 100 g, T = 170 °C, t = 6 h; p = 50 bar)

	Ratio [%]		
	No CO	1.2% CO	6% CO
CO	—	13.2	14.5
CH_4	—	82.4	85.2
CO_2	—	4.3	0.3

Temperature variation

The temperature theoretically influences the rates of the competitive reactions and the adsorption strength of CO. To investigate these combined effects on hydrogenation performance, temperature variation experiments were conducted. Fig. 3 shows BT conversion (left) and selectivity (right) to hydrogenation products at T = 170 °C, 200 °C and 230 °C with 1.2% CO content. At 230 °C, full conversion was reached after 60 min, while 120 min and 6 h were required at 200 °C and 170 °C, respectively. Consequently, all temperatures allow BT hydrogenation with the Ni catalyst in the presence of CO. While the hydrogenation at 170 °C

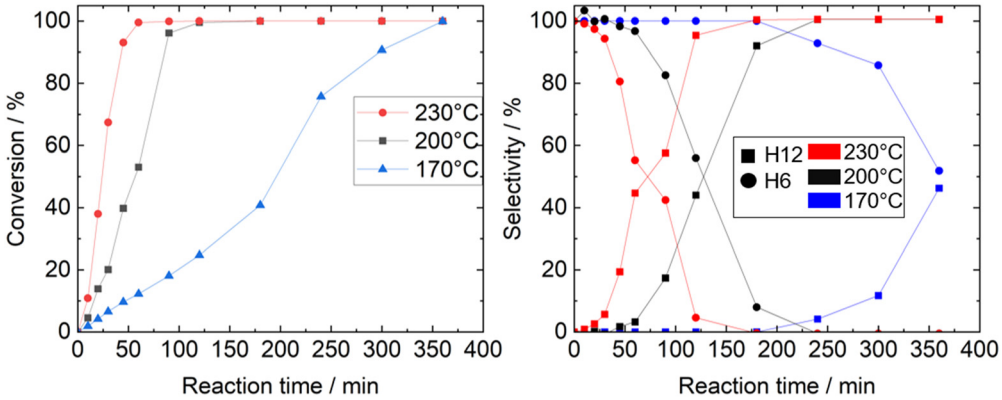

Fig. 3 Conversion (left) and selectivity (right) of benzyltoluene hydrogenation using a commercial nickel catalyst at 170 °C (blue), 200 °C (black) and 230 °C (red) (reaction conditions: Ni/BT ratio 0.045, m_{BT} = 100 g, t = 6 h; p = 50 bar, CO gas fraction 1.2%).

displays a DoH of only 72.2%, the other experiments reach full hydrogenation after 4 h at 200 °C and 3 h at 230 °C, respectively. CO conversion (see Table 2) of 82.4% at 170 °C and almost total conversion at 200 °C with 99.6% and 98.0% at 230 °C are recorded after 6 h reaction time. At 170 °C, as mentioned in the previous section, two distinct kinetic regimes can be identified during the reaction. An initial regime characterized by reduced hydrogenation activity is consistent with strong CO co-adsorption and concurrent CO methanation, which limits hydrogen availability and blocks active sites. From an Arrhenius perspective, this behaviour can be attributed to the relatively high apparent activation energy of aromatic BT hydrogenation compared to the lower activation energy associated with CO methanation and the strong temperature dependence of CO adsorption. Table 2 shows the composition of the C1 components in the gas phase after 6 h reaction time. Higher temperatures lead to a pronounced increase in methanation activity, leading to nearly full conversion of CO at 200 °C and 230 °C.

Schmider *et al.* postulated that at lower temperatures and high hydrogen partial pressure the hydrogenation of unsaturated compounds is favoured over the otherwise thermodynamically favoured CO methanation on Ni surfaces.[52] Furthermore, they reported an increased surface coverage of CO at lower temperatures, leading to site blocking and reduced hydrogen adsorption, which further suppresses methanation as well as the BT conversion in the case of our study.[52] The temperature variation was further conducted with a CO content of 6% and otherwise identical reaction conditions. To obtain insights into the progression of gas phase composition during the experiment gas samples were taken over the course of the experiment (Fig. 4). The respective selectivity plots can be found in the SI (Fig. S1–S3).

At 200 °C, complete conversion of H0-BT and full hydrogenation were achieved within 6 h of reaction time. Increasing the reaction temperature to 230 °C significantly accelerated the process, with full H0-BT conversion after 3 h and complete hydrogenation to H12-BT after 4 h. In contrast, a conversion of only 12.1% was reached at 170 °C after 6 h (final DoH of 6.2%). Nearly complete CO conversion is achieved at 200 °C (X_{CO} = 98.1%) and 230 °C (X_{CO} = 98.9%), whereas only 85% is observed at 170 °C. This behaviour can be attributed to accelerated CO methanation kinetics at elevated temperatures, which enhance CO consumption and partially regenerate the catalyst surface.[53] Furthermore, a temperature of 170 °C seems to be insufficient to provide adequate surface mobility regarding CO desorption while also being too low to promote sufficient CO methanation to liberate surface centres.

Table 2 Composition of the C1 components of the gas phase of benzyltoluene hydrogenation using a commercial nickel catalyst at 170 °C, 200 °C and 230 °C (reaction conditions: Ni/BT ratio 0.045, m_{BT} = 100 g, t = 6 h; p = 50 bar, CO gas fraction 1.2%)

	Ratio [%]		
	170 °C	200 °C	230 °C
CO	13.2	0.4	1.3
CH_4	82.4	99.6	98.0
CO_2	4.3	0	0.8

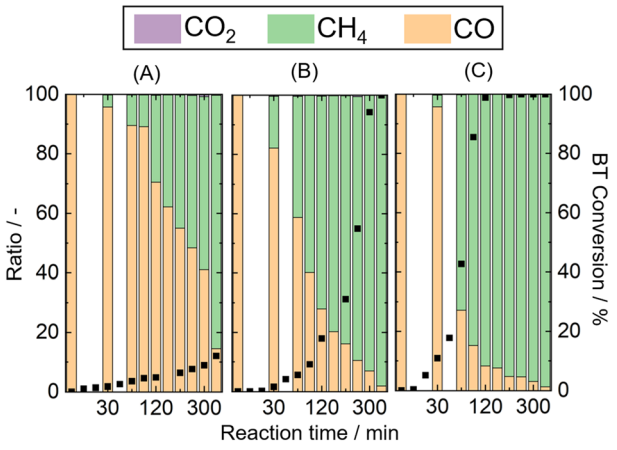

Fig. 4 BT conversion (black) and ratio of the C1 components CO_2 (purple), CH_4 (green) and CO (yellow) of benzyltoluene hydrogenation using a commercial nickel catalyst at 170 °C (A), 200 °C (B), and 230 °C (C) (reaction conditions: Ni/BT ratio 0.045; m_{BT} = 100 g, p = 50 bar, t = 6 h, CO gas fractions 6%).

When increasing the CO concentration from 1.2% to 6%, the hydrogenation is markedly inhibited. This inhibitory effect is more pronounced at lower temperatures, where at 200 °C the reaction time increases by 200% (*i.e.*, the reaction proceeds threefold more slowly), whereas at 230 °C the hydrogenation is only 100% slower (*i.e.*, approximately twofold more slowly). The initial deviation can be attributed to the higher CO concentration, which results in a larger fraction of active sites being blocked by strongly adsorbed CO species. Although the increased temperature accelerates both CO methanation and benzyltoluene hydrogenation, the sustained CO availability maintains a high surface coverage, thereby limiting further improvements in BT conversion despite intrinsically faster hydrogenation kinetics.[54] The subsequent steepening of the conversion profile, after approximately 90 min for the experiment at 200 °C and after 10 min at 230 °C, reflects partial surface reactivation, reinforcing the conclusion that CO acts as a strong inhibitor by competitively blocking active sites on the nickel surface. At lower CO partial pressures, CO conversion is limited by gas–liquid mass transfer and competitive adsorption between CO and H_2 on the catalyst surface.[55]

Regarding the catalyst stability, no loss of active metal or reduction of surface area could be detected (see Table S2). At the beginning of the reaction, the nickel catalyst is still covered by a superficial oxide layer. It was previously reported that this oxide layer is removed under reaction conditions during the hydrogenation.[51] After the reaction, handling of the catalyst under ambient air and subsequent washing, this oxide layer re-forms on the catalyst surface (see Fig. S14 and S15).

Variation of total pressure

Additional experiments at reduced total pressure of 10 bar and 30 bar have been conducted at 200 °C. The CO concentration was kept constant at the beginning of these experiments, while CO partial pressure increased with total pressure accordingly. A decrease in BT conversion was observed with decreasing pressure (Fig. 5, selectivity in Fig. S4–S6). While all experiments reached total conversion of H0-BT, only the 30 bar (DoH ≥99.9% after 6 h) and 50 bar (DoH ≥99.9% after 4 h) experiments achieved full hydrogenation to H12-BT. A DoH of 77.3% was reached in the 10 bar experiment after 6 h reaction time. Alongside the kinetics of BT conversion, the CO conversion was monitored over the reaction time (Fig. 6). About 90% of CO was converted into methane at all pressures after 30 min of operation. This proves the high activity of the Ni catalysts in the competing methanation reaction. At lower pressures, the CO conversion is influenced by gas–liquid transfer processes or by competitive adsorption between CO and H_2 on the catalyst surface.[55] However, at elevated pressures, where gas solubility and partial pressures are sufficiently high, these effects become less pronounced. Consequently, increasing the total pressure beyond this point does not enhance CO conversion, indicating that the surface reaction kinetics or adsorption equilibrium govern the overall reaction rate under these conditions.[56] CO_2 formation by the reverse water-gas shift reaction could not be observed in the experiments, even though methanation produces water as a stoichiometric by-product.

Hydrogenation with multiple impurities

In a subsequent series of experiments, CO_2 was introduced as an additional gas impurity, to investigate its effect during BT hydrogenation with Ni catalysts. As CO_2 constitutes a major product of biomass gasification alongside hydrogen, its concentration was set to 30%, in accordance with values reported in the literature.[57] This resulted in a gas composition of 30% (15 bar) CO_2, 0.6% (0.3 bar) CO and

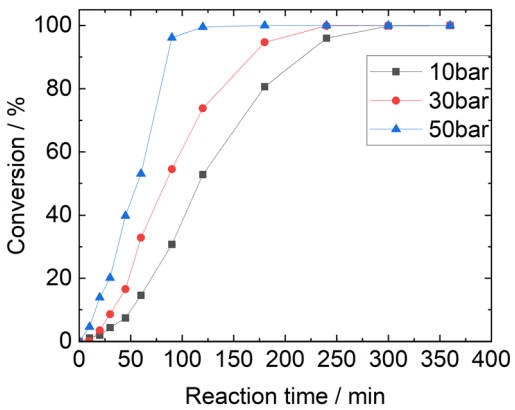

Fig. 5 Conversion of benzyltoluene in hydrogenation using a commercial nickel catalyst at 10 bar (black), 30 bar (red) and 50 bar (blue) (reaction conditions: Ni/BT ratio 0.045; m_{BT} = 100 g, T = 200 °C, t = 6 h, CO gas fraction 1.2%).

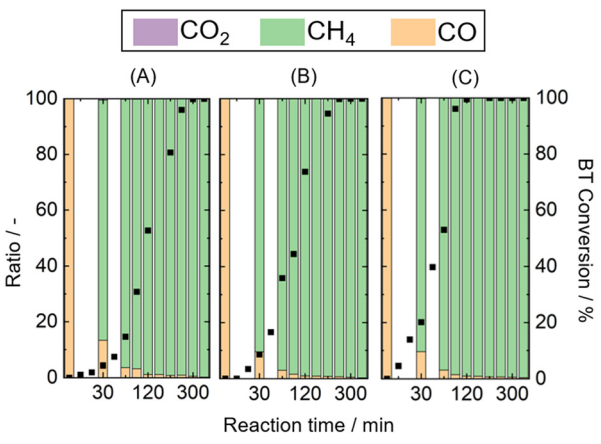

Fig. 6 BT conversion (black) and ratio of the C1 components CO_2 (purple), CH_4 (green) and CO (yellow) of benzyltoluene hydrogenation using a commercial nickel catalyst at 10 bar (A), 30 bar (B) and 50 bar (C) (reaction conditions: Ni/BT ratio 0.045; m_{BT} = 100 g, T = 200 °C, t = 6 h, CO gas fraction 1.2%).

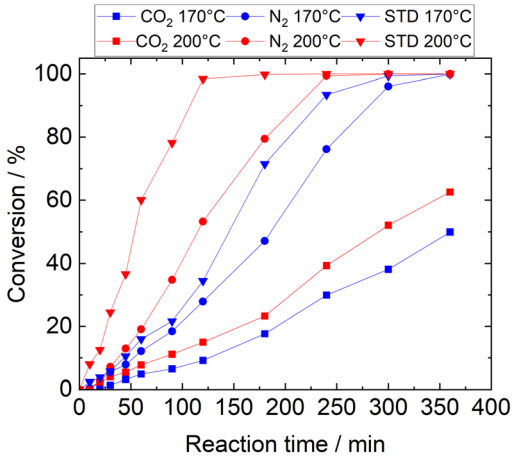

Fig. 7 Conversion of benzyltoluene in hydrogenation using a commercial nickel catalyst at 170 °C (blue), 200 °C (red) and CO_2 and N_2 as additional gases compared to a hydrogenation experiment with CO as the only impurity (reaction conditions: Ni/BT ratio 0.045; m_{BT} = 100 g, p = 50 bar, p_{N_2/CO_2} = 15 bar, t = 6 h, CO gas fraction 0,6%).

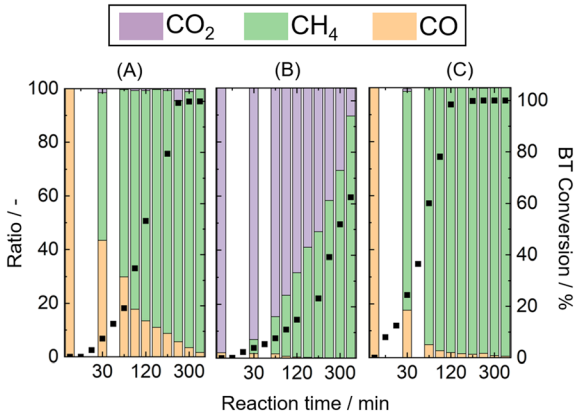

Fig. 8 BT conversion (black) and ratio of the C1 components CO_2 (purple), CH_4 (green) and CO (yellow) in benzyltoluene hydrogenation using a commercial nickel catalyst and N_2 (A) and CO_2 (B) as additional gases, compared to a hydrogenation experiment with CO as the only impurity (C) (reaction conditions: Ni/BT ratio 0.045; m_{BT} = 100 g, p = 50 bar, p_{N_2/CO_2} = 15 bar, T = 200 °C, t = 6 h, CO gas fraction 0,6%).

69.4% (34.7 bar) H_2 at the start of the experiment. The corresponding H0-BT conversion is presented in Fig. 7 (square) at 170 °C and 200 °C and is compared to experiments without CO_2 (Fig. 7, triangle) under otherwise identical reaction conditions (selectivity shown in the SI, Fig. S7, S8, S11 and S12). For the reference experiments without additional CO_2 full conversion of H0-BT after 5 h at 170 °C and 3 h at 200 °C was recorded. Additionally, a DoH of 88.4% was achieved at 170 °C after 6 h, while complete hydrogenation was observed after 4 h at 200 °C. The presence of CO_2 had a pronounced negative impact on the total conversion, resulting in a DoH of only 25.7% at 170 °C. Raising the temperature had only a minimal effect with an increase of DoH to 32.6% at 200 °C. The reduced conversion observed upon the addition of CO_2 could be attributed to multiple parallel effects. Dilution of the feed gas lowers the hydrogen partial pressure and thereby reduces the intrinsic BT hydrogenation rate. Beyond this, CO_2 may influence the reaction indirectly through surface-mediated parallel reactions, such as the reverse water-gas shift reaction, resulting in *in situ* CO formation and its subsequent competitive adsorption on the catalyst surface. Moreover, while CO_2 binds less strongly than CO, its adsorption can partially occupy active sites, thereby limiting H_2 activation and the hydrogenation of BT.[58] To further assess the role of CO_2, additional experiments were conducted in which the 15 bar CO_2 fraction was replaced by N_2, thereby providing a chemically inert reference to isolate purely dilution-related kinetic effects. The results are shown in Fig. 7 (circles). In contrast to the CO_2 experiments, the addition of N_2 results in full conversion after 6 h at 170 °C and after 4 h at 200 °C. Thereby, the DoH reached 62.3% at 170 °C and 84.0% at 200 °C, substantially lower than that in the experiment with pure hydrogen. The reduced degree of hydrogenation observed in the N_2-diluted experiments can be attributed to the lower hydrogen partial pressure, as nitrogen remains chemically inert.[55] This observation is further substantiated by gas phase analysis (see Fig. 8A), which reveals a substantially slower conversion of CO compared to that in the reference experiments (see Fig. 8C). Since the substitution of CO_2 with N_2 resulted in vastly higher BT conversions, it is assumed that CO_2 in an active compound, competed with H_x-BT for active sites and maybe even participated in a parallel reaction. This is further substantiated by the results of the gas phase analysis of the CO_2 substituted experiment (see Fig. 8B). CO_2 is gradually converted into methane over the Ni catalyst. Several mechanistic pathways may contribute to this transformation. One possibility is an associative, formate-mediated route, in which CO_2 is first activated on the surface to form *HCOO species, which undergo stepwise hydrogenation *via* intermediates such as *HCO, *H_2CO, and *CH_3O, ultimately yielding CH_4.[52] Schmider *et al.* reported that CH_4 formation *via* the RWGS pathway is accompanied by an increase in CO partial pressure.[52] In contrast to that, Fig. S13 shows the CO content in ppm over the reaction time for the experiment displayed in Fig. 8. This indicates that CO did not accumulate in the gas phase to a measurable extent. This observation does not exclude transient CO formation at the catalyst surface, but it suggests that any CO formed was rapidly consumed and did not persist as a detectable gas-phase intermediate. Studies on closely related Ni/SiO_2–Al_2O_3 systems further show that the support composition can significantly affect catalyst performance and CO_2 adsorption behaviour, underlining the relevance of support-dependent CO_2 activation on such Ni-based catalysts.[48,49] Accordingly, the present experiments do not allow an unambiguous distinction between a direct CO_2 methanation pathway, an associative formate-mediated route, and an RWGS/CO methanation sequence involving only transiently formed CO. Nevertheless, independent of the

exact mechanistic pathway, CO_2 conversion to methane competes with H_x-BT hydrogenation for hydrogen and catalytically active surface sites, which is consistent with the observed lower hydrogenation rate and reduced DoH.

Hydrogen utilization

Another important consideration is the degree of hydrogen utilization towards the desired purification reaction. Complete hydrogenation of 100 g H0-BT requires 3.29 mol H_2, whereas methanation of 0.3 bar CO (corresponding to a 0.6% CO gas fraction at 50 bar total pressure) consumes only 4.89×10^{-3} mol H_2. This corresponds to a hydrogen utilization of 99.86% with respect to the purification step. An increase in CO content to 0.6 bar (corresponding to 1.2% CO gas fraction at 50 bar) consumes 9.2×10^{-3} mol H_2 with a utilization degree of 99.72%. The highest CO partial pressure in this work was 3 bar (corresponding to 6.0% CO gas fraction at 50 bar) and consumed 4.89×10^{-2} mol H_2, corresponding to a utilization degree of 98.54%. These results indicate that hydrogen losses due to CO methanation are negligible at such low CO concentrations in hydrogen and that the observed acceleration in reaction rate is primarily associated with the removal of CO as a strongly adsorbed catalyst inhibitor, leading to progressive reactivation of the nickel surface. In comparison, the addition of 15 bar CO_2 leads to the consumption of 0.31 mol H_2 during the methanation reaction, reducing the utilization degree to 90.6%. It should be noted, however, that the resulting gas stream constitutes an energy-rich, combustible mixture that can be valorized in downstream processes, offering a potential route for energy recovery that is not available in the original CO_2/CO feed impurities. In summary, while Ni displays clear advantages including low material cost and the absence of irreversible deactivation by CO or CO_2 due to their conversion *via* methanation, which continuously regenerates active surface sites. This behavior represents a limitation for mixed-gas hydrogenation of the LOHC benzyltoluene, as methanation is associated with hydrogen consumption, particularly in gas mixtures containing high concentrations of CO and/or CO_2. Consequently, for typical biomass-derived gas mixtures, an upstream CO_2 removal step is necessary to significantly reduce the CO_2 concentration prior to hydrogenation. From a process-engineering perspective, this requirement is realistic because upstream CO_2 removal is already an established unit operation in industrial hydrogen and syngas processing, with amine scrubbing, physical solvent absorption, and pressure swing adsorption (PSA)-based polishing representing the most relevant options in this context.[59,60] For H_2-rich shifted syngas, MDEA-based amine scrubbing is widely used and reported to achieve roughly 90–99.8% CO_2 capture, depending on process design and optimization.[61] Applied to the feed composition in this study (containing 30 vol% CO_2), such capture levels would lower the residual CO_2 concentration to approximately 3.0 vol% at 90% and up to 0.06 vol% at 99.8% capture rate. However, deeper capture is associated with higher solvent-regeneration duty, additional CO_2 compression work, and larger absorber/stripper equipment.[61] In the optimized MDEA process reported by Antonini *et al.*, the specific equivalent work increased from about 0.585 MJ $kg_{CO_2}^{-1}$ at 90% capture to about 0.681 MJ $kg_{CO_2}^{-1}$ at 99.8% capture, while feasible packed-column designs remained below 15 m packing height but increased substantially toward deeper capture.[61] For pressurized syngas, physical solvents such as Selexol or Rectisol are attractive alternatives for bulk CO_2 removal because they perform well at elevated CO_2 partial pressure and generally require less thermal regeneration than chemical solvents, although they are less suitable for very deep polishing.[62,63] PSA, in contrast, is widely used as a final hydrogen purification step in biomass-to-hydrogen process chain, but is less attractive as the sole front-end option for a stream containing higher CO_2 content.[60] In this context, the practical potential of the investigated Ni catalysts lies in process chains in which CO_2 is removed upstream while residual CO remains, since the present results show substantially stronger inhibition by 30 vol% CO_2 than by 1.2 vol% CO. The corresponding limitation is that the economic advantage of cheap commercial Ni catalysts may be partly offset if very deep CO_2 removal is required to suppress the pronounced CO_2-induced loss in hydrogenation performance, because deeper capture is associated with higher regeneration energy, additional CO_2 compression duty, and larger absorber/stripper equipment.[61]

Conclusion

In this study, a commercially available Ni catalyst was investigated regarding its activity in benzyltoluene (BT) hydrogenation with impure hydrogen containing CO (0.6–6% gas fraction) as well as CO_2 (30% gas fraction). These were chosen as relevant impurities in biomass-derived hydrogen and being known to kinetically inhibit typical noble metal hydrogenation catalysts. CO strongly affected H0-BT conversion and degree of hydrogenation. Complete conversion was still achieved in the absence of CO and at 1.2 vol% CO, although with delayed kinetics and reduced selectivity due to competitive adsorption and parallel CO methanation; 6 vol% CO led to severe inhibition and a pronounced suppression of hydrogenation activity. Additional temperature- and pressure-dependent experiments showed that CO inhibition is largely reversible and governed by surface kinetics. Increasing temperature promoted CO conversion and catalyst surface reactivation, while lowering the pressure from the standard condition of 50 bar reduced H0-BT hydrogenation performance. Since hydrogen consumption by CO methanation remained negligible in the overall balance, the detrimental effect of CO is mainly attributed to temporary blocking of active sites rather than to a substantial loss of hydrogen.

In contrast, CO_2 caused a much stronger deterioration in H0-BT hydrogenation performance. Besides competitive adsorption, the parallel methanation of CO_2 reduced the hydrogen available for H_x-BT hydrogenation and thereby significantly lowered the final degree of hydrogenation and hydrogen utilization. Comparison with N_2-containing reference experiments confirmed that the inhibitory effect of CO_2 cannot be explained by simple dilution alone. Overall, the results demonstrate that Ni catalysts are promising for LOHC-based purification of CO-containing hydrogen streams, while effective upstream CO_2 removal remains necessary for CO_2-rich biomass-derived feeds.

In conclusion, nickel catalysts combine low cost with resistance to irreversible CO/CO_2 poisoning due to continuous surface regeneration *via* methanation; however, this advantage becomes a limitation in mixed-gas hydrogenation because methanation preferentially consumes hydrogen, especially at high CO/CO_2 levels. Therefore, biomass-derived gas streams require upstream CO_2 removal, for example by amine scrubbing, to enable efficient hydrogenation.

Author contributions

LP: data curation, formal analysis, investigation, methodology, visualization, conceptualization, writing – original draft. PS: conceptualization, project administration, supervision.

Conflicts of interest

There are no conflicts to declare.

Abbreviations

BT	Benzyltoluene
H0-BT	Fully dehydrogenated benzyltoluene
H_x-BT	Partially hydrogenated benzyltoluene
*X	Substance X adsorbed on the catalyst surface
DoH	Degree of hydrogenation
H_6	Partially hydrogenated benzyltoluene with a DoH of exactly 50%
H12	Fully hydrogenated benzyltoluene

Data availability

Data for this article is available at the data repository zenodo (https://doi.org/10.5281/zenodo.18656400).

Supplementary information (SI): the SI provides further theoretical background of this study and presents the time-dependent evolution of product selectivity during the hydrogenation experiments. Furthermore, post-mortem analysis of the spent catalyst is presented and compared with the corresponding materials before their use in the reaction. See DOI: https://doi.org/10.1039/d6cy00216a.

Acknowledgements

The authors would like to thank the Federal Ministry of Research, Technology, and Space for funding the BMFTR Junior Research Group FAIR-H2 (grant number FKZ: 03SF0730).

References

1 P. Tavares Borges, E. E. Silva Lora, O. J. Venturini, M. R. Errera, D. M. Yepes Maya, Y. Makarfi Isa, A. Kozlov and S. Zhang, A Comprehensive Technical, Environmental, Economic, and Bibliometric Assessment of Hydrogen Production Through Biomass Gasification, Including Global and Brazilian Potentials, *Sustainability*, 2024, **16**(21), 9213, DOI: 10.3390/su16219213.

2 S. Dasappa, A. M. Shivapuji and M. S. Stanislaus, Green Hydrogen from Biomass Through Gasification—A Carbon Negative Route for Hydrogen Production, in *Climate Action and Hydrogen Economy: Technologies Shaping the Energy Transition*, ed. M. Goel and G. Sen, Springer Nature Singapore, Singapore, 2024, pp. 175–194, DOI: 10.1007/978-981-99-6237-2_11.

3 F. M. Alptekin and M. S. Celiktas, Review on Catalytic Biomass Gasification for Hydrogen Production as a Sustainable Energy Form and Social, Technological, Economic, Environmental, and Political Analysis of Catalysts, *ACS Omega*, 2022, **7**(29), 24918–24941, DOI: 10.1021/acsomega.2c01538.

4 J. Full, S. Merseburg, R. Miehe and A. Sauer, A New Perspective for Climate Change Mitigation—Introducing Carbon-Negative Hydrogen Production from Biomass with Carbon Capture and Storage (HyBECCS), *Sustainability*, 2021, **13**(7), 4026, DOI: 10.3390/su13074026.

5 P. Kundu, S. V. Vineetha, A. Mohan and A. Ravikumar, Bio-Hydrogen Production from Various Waste Resources through Circular Economy: Current Technologies and Future Perspective, *J. Mater. Cycles Waste Manage.*, 2025, **27**(3), 1263–1282, DOI: 10.1007/s10163-025-02183-x.

6 M. Abawalo, K. Pikoń and M. Landrat, Comparative Life Cycle Assessment of Hydrogen Production via Biogas Reforming and Agricultural Residue Gasification, *Appl. Sci.*, 2025, **15**(9), 5029, DOI: 10.3390/app15095029.

7 L. Rosa and M. Mazzotti, Potential for Hydrogen Production from Sustainable Biomass with Carbon Capture and Storage, *Renewable Sustainable Energy Rev.*, 2022, **157**, 112123, DOI: 10.1016/j.rser.2022.112123.

8 S. Khlifi, V. Pozzobon and M. Lajili, A Comprehensive Review of Syngas Production, Fuel Properties, and Operational Parameters for Biomass Conversion, *Energies*, 2024, **17**(15), 3646, DOI: 10.3390/en17153646.

9 T. N. Gebresilasie, F. A. Belete, A. G. Mekonen, K. F. Kahsay and S. K. Abraha, Simulation Based Analysis of Syngas Production from Combined Solid Waste Biomass of Rice Husk Coffee Husk and Sawdust, *Discover Energy*, 2025, **5**(1), 25, DOI: 10.1007/s43937-025-00093-5.

10 Y. Gao, M. Wang, A. Raheem, F. Wang, J. Wei, D. Xu, X. Song, W. Bao, A. Huang, S. Zhang and H. Zhang, Syngas

Production from Biomass Gasification: Influences of Feedstock Properties, Reactor Type, and Reaction Parameters, *ACS Omega*, 2023, **8**(35), 31620–31631, DOI: 10.1021/acsomega.3c03050.

11 N. Faddeev, M. Belichenko, A. Kuriganova and N. Smirnova, Carbon Monoxide Poisoning and Mitigation Strategies for Platinum Catalysts Prepared via Pulse Alternating Current Technique, *J. Electrochem. Sci. Technol.*, 2025, **16**(3), 304–313, DOI: 10.33961/jecst.2024.01032.

12 W. Chen, J. Cao, W. Fu, J. Zhang, G. Qian, J. Yang, D. Chen, X. Zhou, W. Yuan and X. Duan, Molecular-Level Insights into the Notorious CO Poisoning of Platinum Catalyst, *Angew. Chem., Int. Ed.*, 2022, **61**(16), 134, DOI: 10.1002/anie.202200190.

13 A.-Q. Dong, H. Li, H.-M. Wu, K.-X. Li, Y.-K. Shao, Z.-G. Li, S.-H. Sun, W.-C. Wang and W.-B. Hu, Weakening CO Poisoning over Size- and Support-Dependent Ptn/X-Graphene Catalyst (X = C, B, N, n = 1–6, 13), *Rare Met.*, 2023, **42**(4), 1138–1145, DOI: 10.1007/s12598-022-02210-y.

14 W. Ni, T. Wang, F. Héroguel, A. Krammer, S. Lee, L. Yao, A. Schüler, J. S. Luterbacher, Y. Yan and X. Hu, An Efficient Nickel Hydrogen Oxidation Catalyst for Hydroxide Exchange Membrane Fuel Cells, *Nat. Mater.*, 2022, **21**, 804–810, DOI: 10.1038/s41563-022-01221-5.

15 T. Katsumi, H. Noguchi, A. Zemba, D. Sato and S. Kadowaki, The Effects of Initial Temperature and Inert–Gas Addition on the Dynamic Characteristics of Hydrogen–Air Deflagration, *J. Visualization*, 2025, **28**(2), 291–301, DOI: 10.1007/s12650-024-01040-7.

16 I. Navarro-Cárdenas and Á. Martín, Thermodynamic Modelling of Mixtures of Water, Carbon Dioxide and Hydrogen at High Pressure and Temperature for Hydrothermal CO2 Reduction Processes, *Front. Phys.*, 2023, **11**, 1219630, DOI: 10.3389/fphy.2023.1219630.

17 G. Kim and H. Lee, Developing Heterogeneous Catalysts for Reverse Water–Gas Shift Reaction in CO2 Valorization, *Korean J. Chem. Eng.*, 2025, **42**(13), 3101–3112, DOI: 10.1007/s11814-024-00349-1.

18 S. D. Martinez-Boggio, S. S. Merola, P. Teixeira Lacava, A. Irimescu and P. L. Curto-Risso, Effect of Fuel and Air Dilution on Syngas Combustion in an Optical SI Engine, *Energies*, 2019, **12**(8), 1566, DOI: 10.3390/en12081566.

19 M. T. Nguyen, V. G. Bui, H.-Q. Do, P. N. Do, X. B. Nguyen, T. T. Ho and T. N. A. Ho, Effect of Hydrogen-Enriched Syngas and Nitrogen Dilution on Ammonia Deflagration Characteristics at Moderate Pressure, *ACS Omega*, 2025, **10**(25), 27404–27414, DOI: 10.1021/acsomega.5c03002.

20 P. Cavaliere, Hydrogen Separation and Purification, in *Water Electrolysis for Hydrogen Production*, ed. P. Cavaliere, Springer International Publishing, Cham, 2023, pp. 509–541, DOI: 10.1007/978-3-031-37780-8_14.

21 I. Burgers, L. Dehdari, P. Xiao, K. G. Li, E. Goetheer and P. Webley, Techno-Economic Analysis of PSA Separation for Hydrogen/Natural Gas Mixtures at Hydrogen Refuelling Stations, *Int. J. Hydrogen Energy*, 2022, **47**(85), 36163–36174, DOI: 10.1016/j.ijhydene.2022.08.175.

22 Z. Du, C. Liu, J. Zhai, X. Guo, Y. Xiong, W. Su and G. He, A Review of Hydrogen Purification Technologies for Fuel Cell Vehicles, *Catalysts*, 2021, **11**(3), 393, DOI: 10.3390/catal11030393.

23 N. A. Abdul Muin, A. Nwaha Isah, U. A. Asli, A. N. Sadikin, N. Norazahar, M. J. Kamaruddin, M. H. Hassim, H. Wai Shin and N. R. Azman, A Short Review on Various Purification Techniques Suitable for Biohydrogen-Mixed Gases, *J. Energy Saf. Technol.*, 2021, **3**(2), 1–9, DOI: 10.11113/jest.v3n2.52.

24 Y. Kim and H. Yang, Hydrogen Purity: Influence of Production Methods, Purification Techniques, and Analytical Approaches, *Energies*, 2025, **18**(3), 741, DOI: 10.3390/en18030741.

25 A. Król, M. Gajec, J. Holewa-Rataj, E. Kukulska-Zając and M. Rataj, Hydrogen Purification Technologies in the Context of Its Utilization, *Energies*, 2024, **17**(15), 3794, DOI: 10.3390/en17153794.

26 E. Naeiji, A. Noorpoor and H. Ghanavati, Energy, Exergy, and Economic Analysis of Cryogenic Distillation and Chemical Scrubbing for Biogas Upgrading and Hydrogen Production, *Sustainability*, 2022, **14**(6), 3686, DOI: 10.3390/su14063686.

27 A. Krótki, J. Bigda, T. Spietz, K. Ignasiak, P. Matusiak and D. Kowol, Performance Evaluation of Pressure Swing Adsorption for Hydrogen Separation from Syngas and Water–Gas Shift Syngas, *Energies*, 2025, **18**(8), 1887, DOI: 10.3390/en18081887.

28 B. Bong, C. Mebrahtu, D. Jurado, A. Bösmann, P. Wasserscheid and R. Palkovits, Hydrogen Loading and Release Potential of the LOHC System Benzyltoluene/Perhydro Benzyltoluene over S–Pt/TiO_2 Catalyst, *ACS Eng. Au*, 2024, **4**(3), 359–367, DOI: 10.1021/acsengineeringau.4c00003.

29 B. Bong, W. A. Kopp, T. Nevolianis, C. Mebrahtu, K. Leonhard and R. Palkovits, Reaction Equilibria in the Hydrogen Loading and Release of the LOHC System Benzyltoluene/Perhydro Benzyltoluene, *Chem. Eng. Technol.*, 2025, **48**(3), e12002, DOI: 10.1002/ceat.12002.

30 Y. Mahayni, L. Maurer, F. Auer, A. Hutzler, P. Wasserscheid and M. Wolf, Structure Sensitivity of the Low-Temperature Dehydrogenation of Perhydro Dibenzyltoluene on Supported Platinum Nanoparticles, *Catal. Sci. Technol.*, 2024, **14**(18), 5464–5473, DOI: 10.1039/D4CY00032C.

31 K. Alconada, F. Mariño, I. Agirre and V. L. Barrio, Exploring Perhydro-Benzyltoluene Dehydrogenation Using Sulfur-Doped PtMo/Al2O3 Catalysts, *Catalysts*, 2025, **15**(5), 485, DOI: 10.3390/catal15050485.

32 T. Rüde, Y. Lu, L. Anschütz, M. Blasius, M. Wolf, P. Preuster, P. Wasserscheid and M. Geißelbrecht, Performance of Continuous Hydrogen Production from Perhydro Benzyltoluene by Catalytic Distillation and Heat Integration Concepts with a Fuel Cell, *Energy Technol.*, 2023, **11**(3), 2201366, DOI: 10.1002/ente.202201366.

33 H. Jorschick, Ein-Reaktor-Konzept und Mischgashydrierung als Verfahrensvarianten zur Effizienzsteigerung in der LOHC-basierten Wasserstoffspeicherung, *Dissertation*, Friedrich-Alexander-Universität Erlangen-Nürnberg, Erlangen, 2019.

34 K. Inagawa, D. Matsumura, M. Taniguchi, S. Uegaki, T. Nakayama, J. Urano, T. Aotani and H. Tanaka, Development of Hydrogen Oxidation Reaction Catalysts to Overcome CO Poisoning and Elucidation of Reaction Mechanism, *J. Phys. Chem. C*, 2023, **127**(24), 11542–11549, DOI: 10.1021/acs.jpcc.3c02237.

35 M. Niermann, S. Drünert, M. Kaltschmitt and K. Bonhoff, Liquid Organic Hydrogen Carriers (LOHCs) – Techno-Economic Analysis of LOHCs in a Defined Process Chain, *Energy Environ. Sci.*, 2019, **12**(1), 290–307, DOI: 10.1039/C8EE02700E.

36 M. Kerscher, J. H. Jander, J. Cui, L. A. Maurer, P. Wolf, J. D. Hofmann, A. Köksal, H. Zachskorn, F. Auer, P. S. Schulz, P. Wasserscheid, M. H. Rausch, T. M. Koller and A. P. Fröba, Thermophysical Properties of the Liquid Organic Hydrogen Carrier System Based on Benzyltoluene Considering Influences of Isomerism and Dissolved Hydrogen, *Int. J. Hydrogen Energy*, 2024, **77**, 1009–1025, DOI: 10.1016/j.ijhydene.2024.06.131.

37 T. Rüde, S. Dürr, P. Preuster, M. Wolf and P. Wasserscheid, Benzyltoluene/Perhydro Benzyltoluene – Pushing the Performance Limits of Pure Hydrocarbon Liquid Organic Hydrogen Carrier (LOHC) Systems, *Sustainable Energy Fuels*, 2022, **6**(6), 1541–1553, DOI: 10.1039/D1SE01767E.

38 H. Jorschick, M. Vogl, P. Preuster, A. Bösmann and P. Wasserscheid, Hydrogenation of Liquid Organic Hydrogen Carrier Systems Using Multicomponent Gas Mixtures, *Int. J. Hydrogen Energy*, 2019, **44**(59), 31172–31182, DOI: 10.1016/j.ijhydene.2019.10.018.

39 A. Seitz, Y. Sheng, I. Backes, P. Nathrath, D. Weber, T. Franken, R. Felix, A. Rillera, J. Fritsch, M. Bär, T. Retzer and P. Schühle, Phosphate modification of Pd/Al_2O_3 enhances activity and stability in aromatic hydrogenation under CO-contaminated hydrogen, *EES Catal.*, 2026, **4**, 118–133, DOI: 10.1039/d5ey00231a.

40 R. Wang, M. Zhang, J. Zhang and J. Yang, Supported Nickel-based Catalysts for Heterogeneous Hydrogenation of Aromatics, *ChemistrySelect*, 2023, **8**(45), e202302787, DOI: 10.1002/slct.202302787.

41 Z. Wang, C. Dong, X. Tang, X. Qin, X. Liu, M. Peng, Y. Xu, C. Song, J. Zhang, X. Liang, S. Dai and D. Ma, CO-Tolerant RuNi/TiO2 Catalyst for the Storage and Purification of Crude Hydrogen, *Nat. Commun.*, 2022, **13**(1), 4404, DOI: 10.1038/s41467-022-32100-x.

42 H. Sekine, M. Ohshima, H. Kurokawa and H. Miura, Liquid Phase Hydrogenation of Naphthalene in the Presence of CO over Supported Ni Catalyst, *React. Kinet. Catal. Lett.*, 2008, **95**(1), 99–105, DOI: 10.1007/s11144-008-5295-5.

43 T. A. Le, J. K. Kang and E. D. Park, Active Ni/SiO2 Catalysts with High Ni Content for Benzene Hydrogenation and CO Methanation, *Appl. Catal., A*, 2019, **581**, 67–73, DOI: 10.1016/j.apcata.2019.05.020.

44 J. Gao, C. Jia, J. Li, M. Zhang, F. Gu, G. Xu, Z. Zhong and F. Su, Ni/Al2O3 Catalysts for CO Methanation: Effect of Al2O3 Supports Calcined at Different Temperatures, *J. Energy Chem.*, 2013, **22**(6), 919–927, DOI: 10.1016/S2095-4956(14)60273-4.

45 P. Riani, E. Spennati, M. V. Garcia, V. S. Escribano, G. Busca and G. Garbarino, Ni/Al2O3 Catalysts for CO2 Methanation: Effect of Silica and Nickel Loading, *Int. J. Hydrogen Energy*, 2023, **48**(64), 24976–24995, DOI: 10.1016/j.ijhydene.2023.01.002.

46 C. Italiano, J. Llorca, L. Pino, M. Ferraro, V. Antonucci and A. Vita, CO and CO2 Methanation over Ni Catalysts Supported on CeO2, Al2O3 and Y2O3 Oxides, *Appl. Catal., B*, 2020, **264**, 118494, DOI: 10.1016/j.apcatb.2019.118494.

47 H. Ju Jung, H. Jeong, D. Kim, H. Ko, G. Bo Han, B. Jeong, T. Wan Kim and Y.-W. Suh, Metal–Support Interface Engineering of Ni Catalysts for Improved H2 Storage Performance: Grafting Alkyltriethoxysilane onto Commercial Alumina, *Chem. Eng. J.*, 2023, **469**, 143872, DOI: 10.1016/j.cej.2023.143872.

48 P. Riani, I. Valsamakis, T. Cavattoni, V. Sanchez Escribano, G. Busca and G. Garbarino, Ni/SiO2-Al2O3 Catalysts for CO2 Methanation: Effect of La2O3 Addition, *Appl. Catal., B*, 2021, **284**, 119697, DOI: 10.1016/j.apcatb.2020.119697.

49 W. L. Vrijburg, G. Garbarino, W. Chen, A. Parastaev, A. Longo, E. A. Pidko and E. J. M. Hensen, Ni-Mn Catalysts on Silica-Modified Alumina for CO2 Methanation, *J. Catal.*, 2020, **382**, 358–371, DOI: 10.1016/j.jcat.2019.12.026.

50 A. Wodołażski, Modelling of Carbon Monoxide and Carbon Dioxide Methanation under Industrial Condition, in *Biogas – Recent Advances and Integrated Approaches*, ed. A. El-Fatah Abomohra, M. Elsayed, Z. Qin, H. Ji and Z. Liu, IntechOpen, 2021, DOI: 10.5772/intechopen.85170.

51 A. W. Tricker, S. Najmi, E. V. Phillips, K. L. Hebisch, J. X. Kang and C. Sievers, Mechanocatalytic Hydrogenolysis of Benzyl Phenyl Ether over Supported Nickel Catalysts, *RSC Sustainability*, 2023, **1**(2), 346–356, DOI: 10.1039/D2SU00089J.

52 D. Schmider, L. Maier and O. Deutschmann, Reaction Kinetics of CO and CO_2 Methanation over Nickel, *Ind. Eng. Chem. Res.*, 2021, **60**(16), 5792–5805, DOI: 10.1021/acs.iecr.1c00389.

53 J. R. Rostrup-Nielsen, Catalytic Steam Reforming, in *Catalysis: Science and Technology*, ed. J. R. Anderson and M. Boudart, Springer Berlin Heidelberg, Berlin, Heidelberg, 1984, vol. 5, pp. 1–117, DOI: 10.1007/978-3-642-93247-2_1.

54 J. Wei and E. Iglesia, Mechanism and Site Requirements for Activation and Chemical Conversion of Methane on Supported Pt Clusters and Turnover Rate Comparisons among Noble Metals, *J. Phys. Chem. B*, 2004, **108**(13), 4094–4103, DOI: 10.1021/jp036985z.

55 W. Kim, K. M. Kamal, D. J. Seo and W. L. Yoon, Kinetic Study on CO-Selective Methanation over Nickel-Based Catalysts for Deep Removal of CO from Hydrogen-Rich Reformate, *Catalysts*, 2021, **11**(12), 1429, DOI: 10.3390/catal11121429.

56 Y. Yue, T. Wang, M. Sakai and Y. Shen, Particle-Scale Study of Spout Deflection in a Flat-Bottomed Spout Fluidized Bed, *Chem. Eng. Sci.*, 2019, **205**, 121–133, DOI: 10.1016/j.ces.2019.04.031.

57 H. Cay, G. Duman and J. Yanik, Two-Step Gasification of Biochar for Hydrogen-Rich Gas Production: Effect of the Biochar Type and Catalyst, *Energy Fuels*, 2019, **33**(8), 7398–7405, DOI: 10.1021/acs.energyfuels.9b01354.

58 N. D. Nielsen, A. D. Jensen and J. M. Christensen, The Roles of CO and CO2 in High Pressure Methanol Synthesis over Cu-Based Catalysts, *J. Catal.*, 2021, **393**, 324–334, DOI: 10.1016/j.jcat.2020.11.035.

59 D. Jansen, M. Gazzani, G. Manzolini, E. V. Dijk and M. Carbo, Pre-Combustion CO2 Capture, *Int. J. Greenhouse Gas Control*, 2015, **40**, 167–187, DOI: 10.1016/j.ijggc.2015.05.028.

60 J. Lundgren, B. Vreugdenhil, Y. Gynjkhanlou and R. Baldwin, *Biomass Gasification for Hydrogen Production*, IEA Bioenergy, 2025, https://www.ieabioenergy.com/wp-content/uploads/2025/03/IEA-Bioenergy_T33_Bio-H2_Final_v2.pdf.

61 C. Antonini, J.-F. Pérez-Calvo, M. Van Der Spek and M. Mazzotti, Optimal Design of an MDEA CO 2 Capture Plant for Low-Carbon Hydrogen Production — A Rigorous Process Optimization Approach, *Sep. Purif. Technol.*, 2021, **279**, 119715, DOI: 10.1016/j.seppur.2021.119715.

62 D. Jansen, M. Gazzani, G. Manzolini, E. V. Dijk and M. Carbo, Pre-Combustion CO2 Capture, *Int. J. Greenhouse Gas Control*, 2015, **40**, 167–187, DOI: 10.1016/j.ijggc.2015.05.028.

63 T. N. Borhani and M. Wang, Role of Solvents in CO2 Capture Processes: The Review of Selection and Design Methods, *Renewable Sustainable Energy Rev.*, 2019, **114**, 109299, DOI: 10.1016/j.rser.2019.109299.